AFOSR-TR-97-0393

REPORT DOCUMENTATION PAGE

Form Approved
OMB No. 0704-0188

1. AGENCY USE ONLY (Leave blank)	2. REPORT DATE	3. REPORT TYPE AND DATES COVERED
	6/17/97	Final Technical 01 Feb 94-30 Apr 97

4. TITLE AND SUBTITLE

STUDIES OF OPTICAL BEAM PHASE CONJUGATION & ELECTROMAGNETIC SCATTERING PROCESS

5. FUNDING NUMBERS

61102F
2301/CS

6. AUTHOR(S)

ROBERT W. HELLWARTH

7. PERFORMING ORGANIZATION NAME(S) AND ADDRESS(ES)

University of Southern California
Los Angeles, CA 90089

8. PERFORMING ORGANIZATION REPORT NUMBER

9. SPONSORING/MONITORING AGENCY NAME(S) AND ADDRESS(ES)

Air Force Office of Scientific Research - NE
Bolling Air Force Base, Building 410
Washington, D.C. 20332-6448

10. SPONSORING/MONITORING AGENCY REPORT NUMBER

F49620-94-1-0139

11. SUPPLEMENTARY NOTES

12a. DISTRIBUTION/AVAILABILITY STATEMENT

APPROVED FOR PUBLIC RELEASE: DISTRIBUTION UNLIMITED

12b. DISTRIBUTION CODE

13. ABSTRACT (Maximum 200 words)

In this project we have performed both experimental and theoretical studies of nonlinear optical beam interactions in a variety of media. During this reporting period we have (1) extended our set of exact focused-pulse solutions of Maxwell's equations in vacuum, (2) discovered a new two-photon resonance in the fullerene C60, (3) measured excited-state cross-sections in protonic-doped bis-benzothiazole, (4) developed a nonlinear interferometer which measures phase, as well as magnitude, of certain nonlinear optical susceptibilities, and (5) completed our experimental and theoretical demonstration of the first clear example of a strongly-coupled large polaron.

14. SUBJECT TERMS

Focused electromagnetic pulse. Fullerenes. Protonic doping. Interferometry. Large Polaron.

15. NUMBER OF PAGES

4+cover+APPENDICES

16. PRICE CODE

17. SECURITY CLASSIFICATION OF REPORT	18. SECURITY CLASSIFICATION OF THIS PAGE	19. SECURITY CLASSIFICATION OF ABSTRACT	20. LIMITATION OF ABSTRACT
UNCLASSIFIED	UNCLASSIFIED	UNCLASSIFIED	UL

UNIVERSITY OF SOUTHERN CALIFORNIA
Department of Physics and Astronomy
Los Angeles, CA 90089-0484

Dr. R.W. Hellwarth
Professor of Electrical
Engineering and Physics

June 17, 1997

Dr. H. Schlossberg
Air Force Office of Scientific Research
Bolling Air Force Base, Building 410
Washington, DC 20332-6448

Re: Contract No. F49620-94-1-0139
Title: Studies Of Optical Beam Phase Conjugation
and Electromagnetic Scattering Process
Interim Technical Report

Dear Dr. Schlossberg:

Please find enclosed the Interim Technical Report on the Contract No. F49620-94-1-0139 submitted in six copies per the report guidelines.

Sincerely yours,

R.W. Hellwarth

cc. Ofelia Galvan, USC, Dept. of Contracts and Grants, MC 1147
Kim Davis, Bolling AFB, DC 20332-8080

Enclosures

(213)740-4380
(213)740-6653 Fax
hellwart@mizar.usc.edu

1. INTRODUCTION AND PROJECT OBJECTIVES

Nonlinear optics, the study of matter interactions with intense electromagnetic fields, has uncovered surprising and useful physical effects, such as stimulated scattering of light by which an intense monolithic beam can be converted to intense coherent beams of different wavelengths. Recently, interesting processes involving nonlinear optical image-bearing beams have been discovered, such as optical-beam phase conjugation. Optical-beam phase conjugation is the name given to any process which generates, in real time, the time-reversed replica of a complex, image-bearing, optical beam, or which generates other related reflected beams, both monochromatic and polychromatic. Phase conjugation by optical four-wave mixing was conceived earlier in this project, as were such applications of phase conjugation as the corrections image aberrations, brightness enhancement of laser outputs, edge-enhancements of images, automatic steering of beams, and optical spectroscopy by Raman-induced phase conjugation (RIPC). Such nonlinear optical techniques are currently being extended to perform many forms of beam processing, sorting, and routing on picosecond time scales. This project aims at exploring and developing these and other new wave-mixing processes, and the necessary nonlinear materials. Other novel electromagnetic scattering processes which occur at intense optical fields available from lasers are also explored for their scientific and device interest. The approaches taken in this project are both experimental and theoretical.

2. MAJOR ACCOMPLISHMENTS: 12/1/93 to 4/30/97

The major accomplishments of this grant from the last date covered by the previous Technical Report (8/31/96) to the final date of the grant (4/30/97) are described briefly below and more completely in the numbered references and the Appendices I and II attached to this report. The major accomplishments from the beginning of this grant up to 8/31/96 are copied from the three yearly Technical Reports preceeding. These give numbered references to complete descriptions of the work, which references appear in Sections 3 and 4 of this report.

2.1 A new interferometric technique to measure amplitude and phase of nonlinear tensor elements.

We have demonstrated an all-optical method that allows the measurement of the amplitude and the phase of all independent elements of the degenerate four-wave-mixing tensor of an isotropic thin film on a thick substrate. The method employs the interference of the degenerate four-wave-mixing signal from the substrate with that from the film, normalized to other signals generated by the same incident beams. Our observation of a negative real part in every element of $\chi^{(3)}$ at 768 nm of C_{60} supports the existence of a two-photon resonance, suggested by others to exist near 1.3 μm. This research is described in detail in Ref. 3.21 which is attached as Appendix I.

2.2 Observation of the mobility of a large polaron

We completed a series of researches on the nature of photoconduction in n-type cubic $Bi_{12}SiO_{20}$. As a result it became clear that the conduction electrons in this crystal constitute the strongest physical example of a long-postulated theoretical entity, a "large polaron." The arguments leading to this conclusion are given in Pub. 3.22 which is attached as Appendix II. Our results were also presented at the conferences 4.12 and 4.13 below.

2.3 The second electro-optic coefficient of benzene

We completed the first measurement of the "second" electro-optic coeffecient of liquid benzene which is often used as a nonlinear standard. The results are described in Pub. 3.20 and the conference talk 4.14.

MAJOR ACCOMPLISHMENTS: 12/1/93 TO 10/31/94

The major accomplishments of this grant period were as follows.

Atoms for logic: an all-optical image correlator.

During the current period we achieved one long-standing goal: to demonstrate an optical correlator that is fast (can correlate more than one million images per second), high capacity (more than 50,000 pixels per square centimeter of nonlinear (vapor) material), and requires low power (we need only 3 mW for 1 microsecond to correlate a 36 pixel pattern with a pattern of 280 pixels). The nonlinear medium was a simple glass cell containing cesium vapor at 57°C. The images were digital arrays which allow quantitative assessment. We believe that this correlator has/the best overall figure-of-merit of any all-optical image correlator yet demonstrated, and stands as the standard for all-optical correlators.

Details of our device and its performance are given in papers 3.4 and 3.5 listed below. Developments in preceding technology of nonlinear vapor cells are also given in papers 3.8 and 3.11 below.

Nonlinear optical susceptibilities of polymer films and solutions.

We continued our collaborative effort to develop better nonlinear optical polymers with L.R. Dalton and colleagues of the USC chemistry department, and with C.W. Spangler and colleagues at Northern Illinois University. We concentrated our efforts on recently-developed optical polymers that have greatly improved thermal stability and solubility, especially bis-thienyl polyenes. Our results are summarized in papers 3.1, 3.3 and 3.7 listed below.

Nonlinear optics of fullerene films and solutions.

We continued our investigations of the physics of nonlinearities in films and solutions of the cage-molecules C_{60} and C_{70} called "fullerenes". We made an improved experimental determination of the large excited state absorption cross-section of the C_{60} molecule. This cross-section is crucial in the design of optical limiters. Details are given in paper 3.2 below.

We made the first measurement of the dependence on wavelength from 740 to 880 nm, of the nonlinear susceptibility tensor elements of the C_{60} molecule. Both magnitude and phase of these elements were determined as we described in paper 3.5 below.

We also performed a simple model calculation of the hyperpolarizability of the C_{60} molecule. The results are summarized in paper 3.10 below.

New techniques for measurement of nonlinear optical coefficients.

We developed a simple method by which to measure simultaneously the real and imaginary parts of the refractive index of a spatially sinusoidal optical grating as well as its exact location in space relative to the beams that produced it. The theory and experiments are outlined in paper 3.9 below.

Advanced degrees awarded from this project (12/1/93 to 10/31/94)

5.1. Ph.D. degree to Ping Xia. See paper 3.12 above.

5.2. Ph.D. degree to Nansheng Tang. See paper 3.13 above.

Professional personnel supported (12/1/93 to 10/31/94)

6.1. Dr. R.W. Hellwarth

6.2. Dr. J.P. Partanen

6.3. Dr. Ping Xia

6.4. Dr. Nansheng Tang

6.5. Mr. Huapeng Guan

Interactions (12/1/93 to 10/31/94)

The interactions by the members of this project are, in addition to the talks, conferences, workshops, and seminars listed in Section 4, the consulting services performed by Professor Hellwarth for Lawrence Livermore National Laboratory (contact: Dr. Mark Henesian). The subject matter for these consultations were lasers and laser beam interactions.

MAJOR ACCOMPLISHMENTS: 11/1/94 TO 10/31/95

The major accomplishments of this grant period were as follows.

Ultra-high electromagnetic field

During the current period, we achieved the first step in our project to determine the physical limits on the possible strengths of electric and magnetic fields. (The highest fields imaginable to date occur in extreme astronomical situations, such as a neutron star, or in focused laser pulses.) We discovered an exact focused-pulse solution to the classical Maxwell equations in vacuum, which solution gives close to, if not exactly, the strongest electric and magnetic fields possible for a given pulse energy and given upper limit to its frequency spectrum. A brief account of this achievement was given as an invited paper at CLEO '95. (see summary reference 4.7 below and Appendix I.) A full account has been submitted to Phys. Rev. and is included as Appendix II. We are currently working on several schemes to generate these solutions in the laboratory.

Nonlinear optical properties of fullerenes.

In the current period, we achieved more measurements, of improved accuracy, of the absorption cross-section (at 522 nm) of the C_{60} molecule in its lowest excited singlet and triplet states. These cross-sections are the major factors governing the excellent performance of C_{60} as an optical limiter. The results are summarized in Pub. 3.16 which is attached as Appendix III. We are currently extending these measurements to determine the refractive index change caused by excited C_{60} molecules.

Atomic vapors as nonlinear elements.

In the current period, we achieved the first direct measurements of the diffusion coefficients of excited atoms in an inert buffer gas. We measured the diffusion of both cesium and potassium atoms in their lowest excited (4P) levels as they diffused in neon and xenon. The results are given in thesis 3.14 and 3.15 below and in manuscripts being prepared for publication. A brief summary is given in the Digest paper 4.9 which is attached as Appendix IV.

In the current period we also studied a trapped-atom method to eliminate the Doppler broadening which tends to spoil the performance of atomic vapors as nonlinear elements. (See Pubs. 3.4 and 3.6.) Preliminary results were presented in the Digest Summary (4.8 below) which is attached as Appendix V.

Advanced degrees awarded from this project (11/1/94 to 10/31/95)

5.1 Ph.D. degree to D.S. Glassner. See paper 3.14 above.
5.2 Ph.D. degree to Bing Ai. See paper 3.15 above.

Professional personnel supported (11/1/94 to 10/31/95)

6.1 Dr. R.W. Hellwarth
6.2 Mr. Huapeng Guan
6.3 Mr. Bing Ai
6.4 Mr. David Glassner

Interactions (11/1/94 to 10/31/95)

The interactions by the members of this project are, in addition to the talks, conferences, workshops, and seminars listed in Section 4., the consulting services performed by Professor Hellwarth for Lawrence Livermore National Laboratory (contact: Dr. Mark Henesian). The subject matter for these consultations were lasers and laser beam interactions.

MAJOR ACCOMPLISHMENTS: 11/1/95 TO 8/31/96

The major accomplishments of this grant period were as follows.

Ultra-high electromagnetic field

During the current period, we continued our project to determine the physical limits on the possible strengths of electric and magnetic fields. (The highest fields imaginable to date occur in extreme astronomical situations, such as a neutron star, or in focused laser pulses.) We discovered a family of exact focused-pulse solutions to the classical Maxwell equations in vacuum, which solutions give among the strongest electric and magnetic fields yet discovered for a given pulse energy and given upper limit to the frequency spectrum. A full account of four subclasses in this family was submitted to and published in Physical Review. See Publ. 3.18. It is included as Appendix I. We are currently working on several schemes to generate these solutions in the laboratory. We have also begun a collaboration with Professor H. Winful of the University of Michigan Optical Sciences Laboratory to study other subclasses of these solutions.

Nonlinear optical properties of fullerenes

In the current period, we achieved more measurements, of improved accuracy, of both the real and imaginary parts of all independent elements of the nonlinear susceptibility that governs degenerate four wave-mixing in bulk C_{60} over the entire wavelength range of 0.74 to 1.7μm. We observed one two-photon resonance and its decay to a clear asymptotic limit at long wavelengths. A description of our technique and early measurements has been submitted to Physical Review. In the current period, we also investigated the question raised by the well-established five-fold increase in absorption cross-section of C_{60} excited to its lowest triplet state. That question is whether there is a corresponding change in the optical polarizability that accompanies the increased absorption. We find that indeed the excited triplet polarizability is ~5% higher than the ground state. Details are given in the long summary of talk 4.11, and included as Appendix II.

Optical properties of protonic-doped species

We have continued our studies of the nonlinear optical effects of various dopants in liquids and solids. We completed a study of protonic doped bis-benzothiazole, a chromophore commonly used in optical polymers. We found that the absorption cross-sections of the first excited singlet and triplet states of the chromophore were ~1.40% and 11% larger than that of the ground state to which the chromophores returned in ~1.4 ns. Details of these results are found in Publ. 3.17 and attached as Appendix III.

New four-wave mixing interferometer

In this period we completed development of an interferometer capable of measuring both the magnitude and phase of the third-order nonlinear optical polarization density that is responsible for degenerate four-wave mixing. We used this technique successfully to find the complex nonlinear susceptibility of an optical chromophore dissolved in methylene chloride. Details are given in Publ. 3.19

Experimental demonstration of the first clear example of a strongly-coupled large polaron

We completed experimental and theoretical studies of the mobility of electrons photoexcited to the conduction band of the clear insulating n-type cubic sillenite crystal $Bi_{12}SiO_{20}$ (n-BSO). We measured the mobility over the temperature range 300 to 480 K. This was sufficient range to compare with the detailed predictions well-established of polaron theory that has only one undetermined parameter, the band effective mass. Taking that mass to be 2.0 ± 0.1 electron masses gives essentially perfect argument with our results. The extensive checks to establish that we have seen what we claim above are complete and being prepared for publication. A preliminary account of our experimental results is given in the summary published with Conference Talk 4.10.

3. PAPERS AND Ph.D. THESES PUBLISHED FROM THIS PROJECT (12/1/93 TO4/31/97)

3.1 "Bipolar formation and nonlinear optical properties in bis-thienyl polyenes," C.W. Spangler, M.Q. He, J. Laquindanum, N. Tang, J.P. Partanen, and R.W. Hellwarth, Mat. Res. Soc. Symp. Proc. Ser., vol. 138, Electrical, Optical and Magnetic Properties of Organic Solid State Materials, pp. 607-612, December 1993.

3.2 "Excited-state absorption cross-section of C_{60}," N. Tang, H. Guan, J.P. Partanen, and R.W. Hellwarth, Proc. S.P.I.E., vol. 2143, pp. 272-280, January 1994.

3.3 "Studies of optical nonlinearity in bis-thienyl polyenes," N.Tang, J.P. Partanen, and R.W. Hellwarth, J. Laquindanum, L. Dalton, M.Q. He, and C.W. Spangler, S.P.I.E. Symposium Proceedings Series, vol. 2285, Nonlinear Optical Properties of Organic Materials VII, pp. 186-195, July 1994,

3.4 "Optical image processing by an atomic vapour," I. Biaggio, J.P. Partanen, B. Ai, R.J. Knize, and R.W. Hellwarth, Nature, vol. 371, pp. 318-320, September 1994.

3.5 "Nonlinear optical properties of C60 films between 740 and 880 nm," F.P. Strohkendl, R.J. Larsen, L.R. Dalton, R.W. Hellwarth, and Z.H. Kafafi, S.P.I.E. Proceedings, vol. 2285, pp. 186-195, September 1994.

3.6 "Optical correlator that uses cesium vapor," I. Biaggio, B. Ai, R.J. Knize, J.P. Partanen, and R.W. Hellwarth, Optics Lett., vol. 19, pp. 1765-1767, November 1994.

3.7 "The design of new organic materials with enhanced nonlinear optical properties," C.W. Spangler, M. He, E.G. Nickel, J. Laquindanum, L.R. Dalton, N.Tang, and R.W. Hellwarth, Mol. Cryst. Lq. Cryst., vol. 240, pp. 17-23, November 1994.

3.8 "A thin atomic vapor as a nonlinear optical medium," B. Ai, D.S. Glassner, R.J. Knize, and J.P. Partanen, Appl, Phys. Lett., vol. 64, pp. 951-953, February 1994.

3.9 "Phase sweep method for characterization of cw-laser-induced dielectric gratings," P. Xia and J.P. Partanen, Optics Lett., vol. 19, pp. 378-380, March 1994.

3.10 "Polarizability of a free electron gas confined to a spherical shell," R.J. Knize, Optics Comm.. vol. 106, pp. 95-96, March 1994.

3.11 "Enhancement of degenerate four-wave mixing by atom-wall collisions in atomic vapors," B. Ai, D.S. Glassner, and R.J. Knize, Phys. Rev. A, vol. 50, p. 3345-3348, October 1994.

3.12 Thesis: "Study of laser-induced dielectric gratings in nonlinear optical crystals," submitted by Ping Xia (Ph.D., EKE.), December 1993.

3.13 Thesis: "Experimental and theoretical studies of the nonlinear optical response of certain fullerenes, polymers, and glasses," submitted by Nanshen Tang (Ph.D., Physics), August 1994.

3.14 Thesis: "Influences of quenching and inert buffer gases in degenerate four-wave mixing in alkali vapors", submitted by David S. Glassner (Ph.D., Physics), December 1994.

3.15 Thesis: "Degenerate four-wave mixing and image processing in cesium vapor", submitted by Bing Ai (Ph. D., Physics), May 1995.

3.16 "Measurement of the excited-state molecular polarizability of C_{60}", N. Tang, R.W. Hellwarth, and J.P. Partanen, Mat. Res. Soc. Proc., vol. 359, pp. 511-516 (1995).

3.17 "Optical limiting in protonic doped bis-benzothiazole", N. Tang, R. W. Hellwarth, J. Partanen, S. Sun, and L. Dalton, Mat. Res. Soc. Symp. Proc. 374, 225-230 (1995).

3.18 "Focused one-cycle electromagnetic pulses", R.W. Hellwarth and P. Nouchi, Phy. Rev. E 54, 889-895, July (1996).

3.19 "Four-wave mixing interferometer", N. Tang and J.P. Partanen, Optics Lett. 21, 1108-1110, Aug. (1996).

3.20 Thesis: "Picosecond nonlinear optical study of acoustic transinents and excited C_{60} in benzene," submitted by Huapeng Guan (PhD., Physics), December, 1996.

3.21 "Phase-mismatched degenerate four-wave mixing: complex third-order susceptibility tensor elements of C_{60} at 768 nm", F.P. Strohkendl, L.R. Dalton, R.W. Hellwarth, H.W. Sarkas, and Z.H. Kafafi, J. Opt. Soc. Am. B, vol. 14, pp. 92-98 (1997).

3.22 "Band mobility of photoexcited electrons in $Bi_{12}Si0_{20}$," I. Biaggio, R. W. Hellwarth, and J.P. Partanen, Phys. Rev. Lett., vol 78, pp. 891-894 (1997).

4. CONFERENCE TALKS WITH PUBLISHED ABSTRACTS (12/1/93 TO4/31/97)

4.1 "Excited State Absorption of C_{60}," N. Tang, H. Guan, J.P. Partanen, and R.W. Hellwarth, Paper 2143-30, OE Lase 1994, Los Angeles, CA January 25, 1994.

4.2 "Image processing with Cs Vapor," R.J. Knize, I. Biaggio, B. Ai, D. Glassner, J.P. Partanen, and R.W. Hellwarth, Paper 171, Joint April meeting. Published in Bulletin of the American Physical Society, vol. 39, p. 1133 (1994). Paper 171 at the Joint April meeting of the Am. Phys. Soc. and the Am. Ass. of Physics Teachers, Crystal City, Va., 20 April 1994.

4.3 "Fast response time, low power optical correlator using alkali vapors." I. Biaggio, B. Ai, R.J. Knize, J.P. Partanen, and R.W. Hellwarth, Paper CTuT6, Conference of Lasers and Electro-Optics (CLEO) 1994, Anaheim, CA, May 11, 1994. Published in International Quantum Electronics Conference, vol. 9, 1994 OSA Technical Digest Series (Optical Society of America, Washington, D.C. 1994), p. 171-172.

4.4 "Improving the angular response of DFWM in atomic vapors," D.S. Glassner, B. Ai, R.J. Knize, J.P. Partanen, and R.W. Hellwarth, Paper QThJ4, Conference on Lasers and Electro-Optics (CLEO) 1994, Anaheim, CA, May 11, 1994. Published in International Quantum Electronics Conference, vol. 9, 1994 OSA Technical Digest Series (Optical Society of America, Washington D.C., 1994), p. 208.

4.5 "Interferometry in degenerate four-wave mixing," N. Tang, J.P. Partanen, and R.W. Hellwarth, Paper QThJ3, IQEC 1994, Anaheim, CA, May 12, 1994.

4.6 "Nonlinear Phase-mismatch spectroscopy of thin films," F.P. Shrohkendl, L.R. Dalton, and R.W. Hellwarth, Paper JThB7, IQEC 1994, Anaheim, CA, May 12 1994. Reference Abstract by: "title," in International Quantum Electronics Conference, vol. 9, 1994 OSA Technical Digest Series (Optical Society of America, Washington D.C., 1994), p. 163-164.

4.7 "Focused one-cycle optical pulse," R.W. Hellwarth (invited) in Quantum Electronics Conference, vol. 16, 19945 OSA Technical Digest Series (Optical Society of America, Washington D.C., 1995), p. 12.

4.8 "CO_2 laser trap for cesium atoms," T. Takekosh, Jen-Rong Yeh, and R.J. Knize , in Quantum Electronics Conference, vol. 16, 1995 OSA Technical Digest Series (Optical Society of America, Washington D.C., 1995), pp. 68-69.

4.9 "Measurements of excited state diffusion coefficients by degenerate four-wave mixing," D.S. Glassner, B. Ai, and R.J. Knize in Quantum Electronics Conference, vol. 16, 1995 OSA Technical Digest Series (Optical Society of America, Washington D.C., 1995), pp. 131-132.

4.10 "Band mobility of photo-excited electrons in $Bi_{12}SiO_{20}$", I. Biaggio, R.W. Hellwarth, and J. Partanen; Quantum Electronics and Laser Science Conference (QELS), Anaheim, CA, 5 June 1996.

4.11 "The optical polarizability of excited C_{60} molecules," H. Guan, R. W. Hellwarth, J. Partanen, N.Tang; Nonlinear Optics: Materials, Fundamentals, and Applications, Maui, Hawaii, 10 July 1996. Published in 1996 Technical Digest Series, vol. 11, pp. 403-405 (Optical Society of America Washington, D.C. 1996).

4.12 "Band mobility of photoexcited electrons in $Bi_{12}Si0_{20}$," I. Biaggio, R. W. Hellwarth, and J.P. Partanen, Digest of meeting on Photorefractive materials, effects, and devices, Optical Society of America, pp. 52-55 (1995).

4.13 "Mobility of large polarons in $Bi_{12}Si0_{20}$," I. Biaggio, R. W. Hellwarth, and J.P. Partanen, Digest of 3rd European Conference on Applications of Polar Dielectrics, Bled, Slovenia, August 26-29, 1996, p. 160 (1996).

4.14 H. Guan, R. W. Hellwarth, and J.P. Partanen, "determination of the thermo-optic coefficients at constant density at benzane through time-resolved degenerate four-wave mixing," Annual meeting of the Optical Society of America, Rochester, N.Y., Oct. 22, 1996, Paper TuD3 abstracted on p. 102 in Program Digest.

Advanced degrees awarded from this project (11/1/95 to 10/31/96)

None

Professional personnel supported (11/1/95 to 10/31/96)

6.1 Dr. R.W. Hellwarth
6.2 Mr. Huapeng Guan
6.3 Dr. Jouni Partanen
6.4 Dr. Fritz Strohkendl

Interactions (11/1/95 to 10/31/96)

The interactions by the members of this project are, in addition to the talks, conferences, workshops, and seminars listed in Section 4., the consulting services performed by Professor Hellwarth for Lawrence Livermore National Laboratory (contact: Joshua Rothenberg). The subject matter for these consultations were lasers and laser beam interactions.

Appendix I

Phase-mismatched degenerate four-wave mixing: complex third-order susceptibility tensor elements of C_{60} at 768 nm

F. P. Strohkendl and L. R. Dalton

Department of Chemistry, University of Southern California, Los Angeles, California 90089-1062

R. W. Hellwarth

Department of Electrical Engineering, University of Southern California, Los Angeles, California 90089-0484

H. W. Sarkas and Z. H. Kafafi

Optical Sciences Division, Naval Research Laboratory, Washington, D.C. 20375

Received December 2, 1995

We describe and analyze an all-optical method to measure both the magnitude and the phase of each (complex) element of the $\chi^{(3)}$ tensor that determines degenerate four-wave mixing in a thin isotropic film on a thick substrate. We use the method to characterize the $\chi^{(3)}$ tensor of a 10-μm C_{60} film (on a CaF_2 substrate) for 110-fs pulses at 768 nm. Using a fused-quartz plate as the nonlinear standard, we find the two independent Maker–Terhune elements of $\chi^{(3)}$ to have magnitudes $|c_{1221}(-\omega, \omega, \omega, -\omega)| = (0.44 \pm 0.03) \times 10^{-12}$ esu and $|c_{1122}(-\omega, \omega, \omega, -\omega)| = (0.50 \pm 0.03) \times 10^{-12}$ esu and phase angles ϕ_{1221} and ϕ_{1122}, whose magnitudes are $145° \pm 17°$ and $139° \pm 10°$. © 1997 Optical Society of America. [S0740-3224(97)01901-2]

1. INTRODUCTION

In degenerate four-wave mixing (DFWM), three beams of the same frequency ω overlap in a medium to generate either a fourth, or more,[1] new beams, also of frequency ω. At low beam intensities the power in each newly generated beam is proportional to the product of the powers of the three incident intensities, and the constant of proportionality has as a factor the absolute square of an element of a third-order susceptibility tensor, often referred to as $\chi^{(3)}_{\text{eff}}$, or simply $\chi^{(3)}$. As the beam frequency ω is increased to where it approaches or exceeds either (1) the lowest one-photon resonance frequency of the medium or (2) half of the lowest two-photon resonance frequency of the medium, $\chi^{(3)}$ passes from being a positive real number to a complex number that varies in a complicated way with frequency ω. Knowledge of the phase of $\chi^{(3)}$, as well as of its magnitude, is relevant for the understanding of the electronic structure of materials as well as for the estimation of the device potential of a given material. For example, some devices require a large real part of $\chi^{(3)}$, which results in field-induced phase changes, whereas other devices require a large imaginary part, which is related to field-induced absorption.

In general, the third-order susceptibility $\chi^{(3)}$ is defined as a function of four frequency arguments $(-\omega_4, \omega_3, \omega_2, \omega_1)$, where the frequencies ω_1, ω_2, and ω_3 are the frequencies of three input fields that create through nonlinear mixing a signal field with frequency $\omega_4 = \omega_1 + \omega_2 + \omega_3$. For example, third-harmonic generation is related to $\chi^{(3)}(-3\omega, \omega, \omega, \omega)$, whereas DFWM is determined by $\chi^{(3)}(-\omega, \omega, -\omega, \omega)$. The magnitudes and the phases of these two quantities are related only as ω approaches zero. They have not been related for experiments on C_{60} to date. Phase measurements of $\chi^{(3)}$ with third-harmonic generation based on the interference of substrate and thin-film signals have been frequently performed. However, most DFWM experiments have measured the intensity of their signal beams and therefore only the magnitudes of various $\chi^{(3)}$ tensor elements. A number of methods that measure the phase and the amplitude of $\chi^{(3)}(-\omega, \omega, -\omega, \omega)$ have been devised. Examples are the DFWM method by Tang,[2] the phase-conjugate double interferometer,[3] measurement of the DFWM signal strength of a substance in solution versus its concentration,[4] Kerr-gate heterodyne detection,[5] and the z-scan technique.[6] For a given thin film on a thick substrate, none of these methods can separate the contributions from the substrate and the thin film to the observed nonlinear signal. Here we introduce a new method that allows one to compare both the magnitude and the phase of all $\chi^{(3)}$ tensor elements of a given thin film to those of a thick substrate. As an application, we characterize fully the $\chi^{(3)}$ tensor of a polycrystalline C_{60} film on a cubic CaF_2 substrate at 768 nm.

The basis of our method is as follows. In wave mixing, the wave vector $\mathbf{k}_{\text{mix}}$ of an electric polarization-density wave created by the nonlinear medium response may or may not be equal to the wave vector $\mathbf{k}_\omega$ of an optical beam that has frequency ω and satisfies all boundary conditions. If it is not, the output beam generated will be reduced in power by a phase-mismatch factor $F \equiv [\sin(x)/x]^2$ over the case where $\mathbf{k}_{\text{mix}} = \mathbf{k}_\omega$. Here, x

0740-3224/97/010092-07$10.00

$\equiv |\mathbf{k}_{\mathrm{mix}} - \mathbf{k}_\omega| l_\alpha/2$, where l_α is the interaction length of the beams in the medium α. Our method compares the power in a generated fully phase-matched beam ($F = 1$) with the powers of beams that have $F = 1 - \delta$, $0 < \delta \ll 1$, for the thin C_{60} film but $F \approx 10^{-2}$ for the thick CaF_2 substrate. In the fully phase-matched beam the signal-field contributions of film and substrate interfere, according to the phase difference ϕ between their respective $\chi^{(3)}$ elements. We establish the interference and determine ϕ by comparing the power in the phase-matched signal beam ($F = 1$) to the powers in signal beams that originate (a) solely in the C_{60} film ($F = 1 - \delta$) and (b) solely in the substrate ($F = 1$).

In the following, we (1) give a theoretical discussion that relates the observed signal fields to the $\chi^{(3)}$ tensor components of thin film and substrate and derives their relative phase, (2) demonstrate our method experimentally in a C_{60} film, and (3) give a discussion of the results that leads, because of redundancies and consistency checks inherent in our method, to corrections of the long-pulse $\chi^{(3)}$ values of fused silica appropriate for short pulses (~110 fs).

2. THEORY

We analyze the various beams radiated at frequency ω by the nonlinear polarization density created by three beams (of frequency ω) incident upon a thin film on a thick substrate. The z axis is chosen normal to the sample. The three incident beams, called 1, 2, and 3 in Fig. 1, are arranged in the so-called forward-four-wave mixing geometry and have wave vectors (a, a, b_α), $(-a, a, b_\alpha)$, and $(-a, -a, b_\alpha)$, respectively. Here the subscript α takes the values a, f, s, or q for air, film, substrate, or fused quartz. We assume that $b_a \gg a$. The incident beams give rise to $\mathrm{Re}[\mathbf{P}_f^{(3)}(\mathbf{r})\exp(-i\omega t)]$, a nonlinear polarization density, at space–time points $(\mathbf{r}, t)$ that generates nine new beams, labeled 4 through 12 in Fig. 1. Beam 4 is the only signal beam that is perfectly phase matched. By measuring the strengths of some of these beams (for different combinations of incident polarization states) relative to a beam generated by the substrate alone, and relative to a standard fused-silica quartz plate, we are able to deduce both the magnitude and the phase of each element of the complex fourth-rank nonlinear susceptibility tensor $\overleftrightarrow{\chi}^f(-\omega, \omega, \omega, -\omega)$ of an isotropic thin film. We express the total optical electric-field vector at $(\mathbf{r}, t)$ in the film as $\mathrm{Re}[\mathbf{E}_\omega^f \exp(-i\omega t)]$, where the complex electric-field amplitude is understood to contain any spatial dependencies such as the superposition of several beams, i.e., $\mathbf{E}_\omega^f \equiv \mathbf{E}_\omega^f(\mathbf{r})$. Then, using the convention of Maker and Terhune,[7] we write

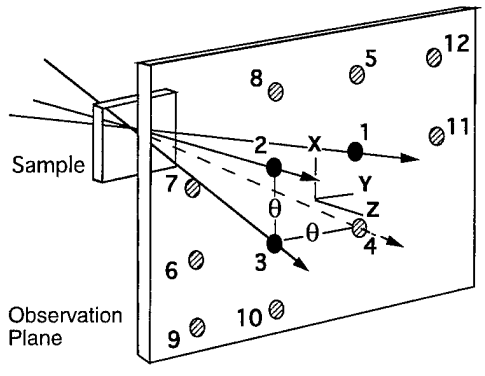

Fig. 1. Beam geometry for degenerate forward-four-wave mixing. Three beams, labeled 1, 2, and 3, copropagate nearly collinearly along the z axis. The angle of intersection in air between beams 1 and 2, and 2 and 3, is denoted by θ. The sample normal is parallel to the z axis. The three incident beams intersect inside the sample and generate, because of third-order nonlinear optical interaction, nine signal beams that are labeled 4–12 in a plane, which we call the observation plane, parallel to the sample. Beam 4 is the phase-matched signal beam; beams 5–12 are non-phase-matched.

$$\mathbf{P}_f^{(3)} = 3\overleftrightarrow{\chi}^f(-\omega, \omega, \omega, -\omega) : \mathbf{E}_\omega^f \mathbf{E}_\omega^f \mathbf{E}_\omega^{f*}, \tag{1}$$

where $\overleftrightarrow{\chi}^f$ is a complex fourth-rank tensor, whose elements we discuss below. When the frequency arguments of $\overleftrightarrow{\chi}^f$ are omitted, they are assumed to be $(-\omega, \omega, \omega, -\omega)$ as in Eq. (1). Note that in the Maker and Terhune definition a factor (1/4) on the right-hand side of Eq. (1) that stems from the multiplication of terms of the form $\mathrm{Re}[\mathbf{E}_\omega^f \exp(-i\omega t)]$ is absorbed into $\overleftrightarrow{\chi}^f$. We will approximate the total complex electric-field amplitude in the air, the film, the substrate, or in the fused-silica reference by

$$\mathbf{E}_\omega^\alpha = \sum_j \mathbf{E}_j^\alpha \exp(i\mathbf{k}_j^\alpha \cdot \mathbf{r}), \tag{2}$$

where the sum is over both incident and generated beams and α refers to the medium in which the field is observed. In the absence of any nonlinear interaction, Eq. (2) is an exact solution of Maxwell's equations with position-independent $\mathbf{E}_j^\alpha$. To solve Maxwell's equations for the generated beams 4 to 12, we will find it sufficient to use the slowly varying envelope approximation or SVEA for $\mathbf{E}_j^\alpha$ ($j = 4$ to $j = 12$), and we assume that the incident-beam amplitudes $\mathbf{E}_j^\alpha$ ($j = 1$ to $j = 3$) are unaltered by the nonlinear interaction.

Consider the SVEA equation for beam 5 (this is of the most general form we will encounter):

$$\frac{\partial \mathbf{E}_5^\alpha}{\partial z} = i\,\frac{12\pi\omega}{n_\alpha c}\,\overleftrightarrow{\chi}^\alpha : \mathbf{E}_1^\alpha \mathbf{E}_2^\alpha \mathbf{E}_3^{\alpha *} \exp(i\Delta k_5^\alpha z), \tag{3}$$

where the wave-vector mismatch Δk_5^α follows from $|\mathbf{k}_5^\alpha| = n_\alpha \omega/c$ and

$$\mathbf{k}_5^\alpha = \mathbf{k}_1^\alpha + \mathbf{k}_2^\alpha - \mathbf{k}_3^\alpha - \Delta k_5^\alpha \hat{\mathbf{z}}, \tag{4}$$

which is required by boundary conditions. Here n_α is the refractive index of the medium α. A nonzero wave-vector mismatch gives rise to phase-mismatch factors $F < 1$ described in Section 1. The term on the right-hand side of Eq. (3) is the only term, from a larger number of terms, for which $|\Delta k_5^\alpha| \ll a$. The other terms are neglected.

In order to estimate the phase-mismatch factor F, we derive a relation between the external beam angle in air, θ (see Fig. 1), and the wave-vector mismatch, Δk_5^α. The beam angle is

$$\theta = \tan^{-1}\frac{2a}{\sqrt{b_a^2 + a^2}} \approx 2ac/\omega. \tag{5}$$

From Eq. (4) one sees that for beam 5 the wave-vector inside a medium α is given by $\mathbf{k}_5^\alpha = (a, 3a, b_5^\alpha)$, which is determined from

$$(k_5^\alpha)^2 = 10a^2 + (b_5^\alpha)^2 = (k_1^\alpha)^2 = 2a^2 + b_\alpha^2 = n_\alpha^2\omega^2/c^2. \tag{6}$$

We approximate b_α by $n_\alpha b_a$, as our angle of incidence is close to normal. Comparing Eq. (6) with Eq. (4), one sees that, for beam 5, the wave-vector mismatch is

$$\Delta k_5^\alpha = b_5^\alpha - b_\alpha = 4a^2c/(n_\alpha\omega) \approx \theta^2\omega/(n_\alpha c). \tag{7}$$

Note also that in our symmetric beam geometry the wave-vector mismatch for beams 5 and 6 is equal.

In our experiments the thickness of the C_{60} film l_f is 10 μm, the refractive index $n_f = 2.0$,[8] $\theta = 2.86°$, and $\lambda = 768$ nm, so that the phase-mismatch angle $x = \Delta k_5^f l_f/2 = 0.05$ and the phase-mismatch factor F is well approximated by 1. However, if we recalculate this angle for the substrate where the refractive index $n_s = 1.43$ and the thickness l_s is 1 mm, we find $\Delta k_5^s l_s/2 \approx 7.13$. From Eq. (3) we see immediately that the phase-mismatch factor F reduces the substrate signal in beam 5 to 1% of what its value would be were $\Delta k_5^s = 0$. We varied the incident-beam angle θ with the sample being the pure substrate without film and found the ratio of the power generated in beam 5 to the power generated in beam 4 (for which the wave-vector mismatch, Δk, is identically zero) to be predicted to within experimental accuracy using Eq. (7) in Eq. (3).

The field generated in phase-matched beam 4 obeys

$$\frac{\partial \mathbf{E}_4^\alpha}{\partial z} = i\frac{12\pi\omega}{n_\alpha c}\overleftrightarrow{\chi}^\alpha : \mathbf{E}_1^\alpha\mathbf{E}_3^\alpha\mathbf{E}_2^{\alpha *}, \tag{8}$$

where $\alpha = f$, s, or q for the film, substrate, or quartz plate, respectively.

In this paper we will study only the signals generated in beam 4, 5, or 6. With the substrate phase mismatch calculated above and with the $\chi^{(3)}$ values that we obtain, we find it consistent to neglect the substrate contributions to beams 5 and 6. They alter these beam powers by less than 1%. That is, we assume that the SVEA equation for beam 6 in the film may be written as

$$\frac{\partial \mathbf{E}_6^f}{\partial z} = i\frac{12\pi\omega}{n_f c}\overleftrightarrow{\chi}^f : \mathbf{E}_2^f\mathbf{E}_3^f\mathbf{E}_1^{f *}, \tag{9}$$

with negligible contribution from the substrate.

Note the differences among Eqs. (3), (8), and (9); we exploit these to advantage. All the beam-overlap corrections are the same for Eqs. (3), (8), and (9), making comparisons among their corresponding signal strengths more accurate than for other signal beams generated, as beams 7 through 12 have only two of the incident beams in the right-hand side of their SVEA equation. Therefore beam-overlap corrections are different among beams 7 through 12, and beam ratios become less accurate for interpretation.

When all beams have the same frequency ω in isotropic media (such as the polycrystalline C_{60} film or the fused-quartz reference plate), the nonlinear polarization density (1) has the particularly simple form

$$\mathbf{P}_\alpha^{(3)} = 3c_{1221}^\alpha\mathbf{E}_\omega^*\mathbf{E}_\omega \cdot \mathbf{E}_\omega + 6c_{1122}^\alpha\mathbf{E}_\omega\mathbf{E}_\omega \cdot \mathbf{E}_\omega^*, \tag{10}$$

where again $\alpha = f$, s, or q for film, substrate, or quartz plate. The complex coefficients c_{1221} and c_{1122} are called the two independent elements of the tensor $\overleftrightarrow{\chi}^\alpha$ in Eqs. (3), (8), and (9). Their frequency arguments are understood to be $(-\omega, \omega, \omega, -\omega)$. Here, following the notation of Maker and Terhune,[7] we use the letter c instead of χ for the tensor components of $\overleftrightarrow{\chi}$. When all incident-beam polarizations are parallel so that $\mathbf{E}_\omega = \hat{\mathbf{x}}E$, a polarization density $\mathbf{P}^{(3)}$ parallel to the field is generated by Eq. (10), whose scalar amplitude is often written $3c_{1111}E^2E^*$, i.e., $c_{1111} = c_{1221} + 2c_{1122}$. Note that here again the total field amplitude, E, is understood to contain any spatial dependencies such as those that arise from the superposition of several beams. For cubic media such as the CaF_2 substrate, $\overleftrightarrow{\chi}^\alpha$ has three independent tensor components. We will not elaborate on these here because they have never been measured and we do not know the orientation of the cube axes in our substrate. The CaF_2 substrate signals will serve simply as an intermediary to the normalization of the C_{60} elements to those of fused quartz, which we know.

In order to calculate the observed signal fields in air after they leave the sample, we correct for Fresnel reflections by assuming that the electric-field amplitude of any beam is multiplied by the Fresnel factor $t_{\alpha\beta}$ in passing from a medium with refractive index n_α to one of index n_β:

$$t_{\alpha\beta} = \frac{2n_\alpha}{n_\alpha + n_\beta}. \tag{11}$$

Multiple reflections are not taken into account. Negligible errors are expected from this approximation since the fraction of the beam power reflected from the C_{60}–substrate interface is less than 3% and since the round-trip time in the 10-μm-thick film is longer than the pulse duration. Here α, β will take the values a (air), f (film), s (substrate), and q (fused quartz).

In the following solutions of Eqs. (8)–(10) we call the beam amplitudes in air just before the sample $\mathbf{E}_j$ ($j = 1, 2, 3$), and we call the generated beam amplitudes in air after the sample $\mathbf{E}_{jL}$ ($j = 4, 5, 6$). Then the solution of Eq. (3) gives directly

$$\mathbf{E}_{5L} = i12\pi\omega l_f[c_{1221}^f\mathbf{E}_3^*\mathbf{E}_2 \cdot \mathbf{E}_1 + c_{1122}^f(\mathbf{E}_1\mathbf{E}_2 \cdot \mathbf{E}_3^* + \mathbf{E}_2\mathbf{E}_1 \cdot \mathbf{E}_3^*)]t_{af}^3t_{fs}t_{sa}/cn_f. \tag{12}$$

The solution of Eq. (9) gives

$$\mathbf{E}_{6L} = i12\pi\omega l_f[c_{1221}^f\mathbf{E}_1^*\mathbf{E}_2 \cdot \mathbf{E}_3 + c_{1122}^f(\mathbf{E}_2\mathbf{E}_3 \cdot \mathbf{E}_1^* + \mathbf{E}_3\mathbf{E}_2 \cdot \mathbf{E}_1^*)]t_{af}^3t_{fs}t_{sa}/cn_f. \tag{13}$$

These two equations relate signals in beams 5 and 6 to the magnitudes of the independent tensor elements of the C_{60} film. The solution of Eq. (8), which contains film and substrate contributions, gives

$$\mathbf{E}_{4L}^{fs} = i12\pi\omega\{[c_{1221}^{f}\mathbf{E}_2^*\mathbf{E}_1 \cdot \mathbf{E}_3 + c_{1122}^{f}(\mathbf{E}_1\mathbf{E}_3 \cdot \mathbf{E}_2^* + \mathbf{E}_3\mathbf{E}_1 \cdot \mathbf{E}_2^*)]l_f t_{af}^3 t_{fs} t_{sa}/cn_f + \overleftrightarrow{\chi}^{s} : \mathbf{E}_1\mathbf{E}_3\mathbf{E}_2^* l_s t_{af}^3 t_{fs}^3 t_{sa}/cn_s\}. \quad (14)$$

In this case the signal power in beam 4 contains an interference term between the complex film and substrate terms. We obtain the magnitudes of the substrate $\chi^{(3)}$ coefficients by observing the signal in beam 4 from the substrate alone, which from Eq. (8) has amplitude

$$\mathbf{E}_{4L}^{s} = i12\pi\omega\overleftrightarrow{\chi}^{s} : \mathbf{E}_1\mathbf{E}_3\mathbf{E}_2^* l_s t_{as}^3 t_{sa}/cn_s, \quad (15)$$

The ratio of this signal to that from the fused-quartz plate alone is used to determine the substrate $\chi^{(3)}$. From Eq. (8) the fused-quartz plate alone produces a field in beam 4:

$$\mathbf{E}_{4L}^{q} = i12\pi\omega[c_{1221}^{q}\mathbf{E}_2^*\mathbf{E}_1 \cdot \mathbf{E}_3 + c_{1122}^{q}(\mathbf{E}_1\mathbf{E}_3 \cdot \mathbf{E}_2^* + \mathbf{E}_3\mathbf{E}_1 \cdot \mathbf{E}_2^*)]l_q t_{aq}^3 t_{qa}/cn_q. \quad (16)$$

The phase angle ϕ_{ijkl} of the thin-film tensor component c_{ijkl}^{f} relative to the substrate tensor element c_{ijkl}^{s} can be derived from experiment by measuring (a) the power in beam 4 for the thin-film sample, $S_4(f, s) \propto |c_{ijkl}^{f} + \gamma c_{ijkl}^{s}|^2$, γ = const., (b) the power in the non-phase-matched beam p for the thin-film sample, $S_p(f) \propto |c_{ijkl}^{f}|^2$, and (c) the power in beam 4 generated by the substrate only, $S_4(s) \propto |c_{ijkl}^{s}|^2$. The beam number p can take the value of either 5 or 6 or both, depending on the polarization state of beams 1, 2, and 3. The correct assignment of p can be derived from Eqs. (12) and (13) by substituting the polarization vectors for the fields and requiring that the same thin-film tensor component generates signals in beams 4 and p. In the case of ϕ_{1111} and ϕ_{1122} a single polarization configuration of beams 1, 2, and 3 suffices. In the case of ϕ_{1221} two different polarization configurations are required. For the correct assignment of p, see also Table 1. The magnitude of the phase angle ϕ_{ijkl} can then be derived from

$$S_4(f, s) = S_p(f) + \xi^2 S_4(s) + 2\xi\sqrt{S_p(f)S_4(s)}\cos(\phi_{ijkl}), \quad (17)$$

where $\xi \equiv (t_{af}t_{fs}/t_{as})^3$, which takes in our case, C_{60} on CaF_2, the value 0.843.

3. EXPERIMENT

Experiments were performed on a polycrystalline (10 ± 0.5)-μm-thick C_{60} film on a 1-mm-thick cubic CaF_2 substrate of unknown orientation. A piece of fused silica of effective thickness (1.46 ± 0.07) mm served as a reference. Beams were derived from a mode-locked femtosecond Ti:sapphire oscillator with a highly stable amplifier operating at 20 Hz, which has been described elsewhere.[9] The center wavelength λ was 768 nm, and the spectral width, 10 nm, was close to transform limited. The pulse duration (intensity full width at half-maximum, FWHM) derived from second-harmonic autocorrelations at the sample location, as well as from Fig. 2, was (110 ± 2) fs, assuming a sech^2 shape for the temporal intensity profile of the pulses. A single beam was split into three beams of similar intensity. These beams, beams 1, 2, and 3 of Fig. 1, passed through a single achromatic lens of focal length 50 cm such that they intersected in the focal plane of the lens. The transverse intensity beam profile in the focal region had a diameter of 150 μm (FWHM). The beam intersection angle θ is 2.9 ± 0.2°. The maximum total intensity at the sample was 20 GW/cm^2. The polarization state of each beam was controlled with zeroth-

Table 1. Powers S_4, S_5, and S_6 Generated in Beams 4, 5, and 6 of Fig. 1 for Various Polarizations of the Input Beams 1, 2, and 3[a]

	Polarization Geometry		a $\frac{S_5(f,s)}{S_4(q)}$	b $\frac{S_6(f,s)}{S_4(q)}$	c $\frac{S_4(s)}{S_4(q)}$	d $\frac{S_4(f,s)}{S_4(q)}$
a	↑	→	1.34 ± 3%	1.14 ± 5%	7.22×10^{-2} ± 8%	1.00 ± 4%
	↑		$\left[\frac{1122}{1122}\right]$	$\left[\frac{1221}{1122}\right]$	$\left[\frac{xxyy}{1122}\right]$	$\left[\frac{1122}{1122}\right]$
b	↑	↑	1.05 ± 4%	1.46 ± 6%	9.93×10^{-2} ± 6%	1.04 ± 6%
	→		$\left[\frac{1221}{1122}\right]$	$\left[\frac{1122}{1122}\right]$	$\left[\frac{xxyy}{1122}\right]$	$\left[\frac{1122}{1122}\right]$
c	↑	↑	1.31 ± 2%	1.29 ± 3%	0.235 ± 4%	0.73 ± 2%
	↑		$\left[\frac{1111}{1111}\right]$	$\left[\frac{1111}{1111}\right]$	$\left[\frac{1111}{1111}\right]$	$\left[\frac{1111}{1111}\right]$
d	→	↑	1.60 ± 7%	1.65 ± 7%	0.132 ± 5%	0.77 ± 8%
	↑		$\left[\frac{1122}{1221}\right]$	$\left[\frac{1122}{1221}\right]$	$\left[\frac{xyyx}{1221}\right]$	$\left[\frac{1221}{1221}\right]$

[a] The polarization geometries shown give the polarizations for beams 1, 2, and 3 in the same order as these beams are shown in the observation plane in Fig. 1. The powers are normalized to the power $S_4(q)$ of beam 4 generated by the fused-quartz plate for the same polarizations. The arguments (f, s) and (s) indicate signals from film-on-substrate and substrate alone. The rows and columns of the table are each labeled by a, b, c, and d so that a single table entry can be referred to elsewhere by matrix notation; e.g., (c, b) refers to the entry 1.29 ± 3%. The brackets below each table entry contain the space indices of the $\chi^{(3)}$ tensor element governing the generated beam written over the space indices of the tensor element of fused quartz responsible for the normalization signal.

order quartz half-wave plates and subsequent calcite polarizers. The polarizers were the last optical elements passed through by the beams before hitting the sample to ensure high polarization purity at the sample. Beams 1 and 3 could be independently delayed with a computer-controlled delay line. The temporal beam overlap was optimized with two-beam autocorrelation signals and was within ±5 fs of the optimum. Spatial beam overlap was achieved with a pinhole of 50-μm diameter. An indexed holder for the sample and the pinhole established sample coordinates relative to the pinhole, which allowed (a) putting the thin film in the plane of optimum spatial beam overlap and (b) repeatable sample positioning. All experiments were performed in a thin-film region of ~0.3-mm diameter. An aperture in the observation plane of Fig. 1 is used to select single signal beams for detection. This aperture is large enough to block all beams emerging from the sample and can be translated in x and y directions. A lens after the aperture is positioned such that it images the interaction region in the sample onto a 4 mm × 4 mm silicon detector. We measure all beam powers emerging from the sample simply by translating the aperture in the observation plane.

Often when one mixes three simultaneous write pulses to generate a fourth signal pulse, the delay in time of one of the write pulses still allows the observation of the signal pulse. The delayed signal arises from a transient remainder of an initial excitation grating produced by two earlier write pulses. Much has been learned from studying these transients. However, we failed to detect these transients in the C_{60} film, the CaF_2 substrate, and the fused-quartz standard at our working intensity. Typical signals versus the time of delay of one of the three incident beams are shown in Fig. 2. Note that the C_{60} signals in beams 5 and 6 are equal, as expected for the all-parallel polarization geometry. The C_{60} signal in strictly phase-matched beam 4 is smaller than in non-phase-matched beams 5 and 6. This clearly indicates destructive interference between the thin-film and the substrate signal fields. Note that the absence of any transient signals makes the analysis in terms of a $\chi^{(3)}$ tensor appropriate.

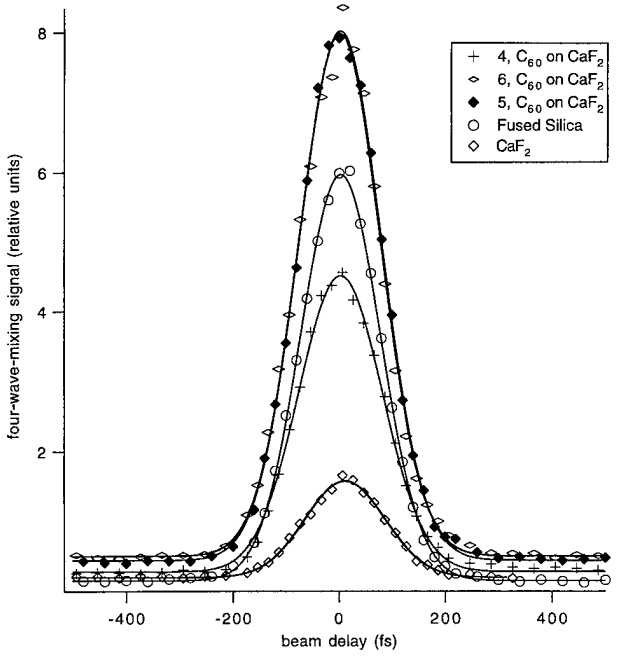

Fig. 2. Degenerate four-wave mixing signals for all-parallel beam polarizations versus beam delay. The signals in beams 4, 5, and 6 emerging from the thin-film sample (C_{60} film on a CaF_2 substrate) and the signals in beam 4 from the pure CaF_2 substrate and the fused-silica standard are shown. Beam 3 was delayed for signals in beams 4 and 6. Beam 2 was delayed for signals in beam 5. All data sets are fit to Gaussians to guide the eye. Note that for the thin-film sample the signal in phase-matched beam 4 is smaller than in non-phase-matched beams 5 and 6. This demonstrates destructive interference between thin-film and substrate signals. Note also that the thin-film signals in beams 5 and 6 are equal, as expected for the parallel polarization configuration.

Each measurement series (which contained measurements of signal beams 4, 5, and 6 for the thin-film sample and measurement of beam 4 for a film-free region of the substrate) started and ended with measurements of beam 4 in fused silica. The fused-silica measurements were used to estimate uncertainties in our experiments that were due to instrument drift as well as to normalize the $\chi^{(3)}$ values of the thin film and the substrate. To obtain a single signal trace, we averaged each data point shown in Fig. 2 over 20 shots. Acquisition of a single signal trace takes ~1 min. To ensure that we were measuring the third-order susceptibility, we checked the intensity dependence of the thin-film signal over three orders of magnitude in signal strength with total beam intensities at the sample up to twice our usual working intensity. We confirmed the intensity dependence I^x to be cubic with $x = 3.0 \pm 0.1$. At five times our working intensity, probing in a different region of our sample, we noticed the appearance of delayed signals and possibly sample damage detected through an increase in the signal background. Care was taken to avoid such high-intensity conditions in our experiments. The comparison of signals from the sample region in which we performed the experiments reported here to signals from other sample regions gave no indication of any sample damage that was due to beam exposure. Our results for thin-film and substrate signal powers normalized by the corresponding phase-matched fused-silica reference signal are shown for four different polarization geometries in Table 1.

4. EVALUATION AND DISCUSSION

Using the 16 data numbers in Table 1, we calculate here the magnitudes and the phases for all nonzero $\chi^{(3)}$ tensor elements of the thin polycrystalline C_{60} film, and we perform consistency checks made possible by multiple independent measurements of c_{1122} and c_{1221} coefficients of the C_{60} film. In this process we will use the fact that the c_{1122} coefficient of the thin film occurs in polarization geometries a, b, and d of Table 1 and can therefore be used to determine the ratio c_{1122}/c_{1221} for fused silica relevant for short pulses (110 fs). We also estimate small (3%) corrections to the best characterized $\chi^{(3)}$ tensor element of

fused silica, c_{1221}, appropriate for our short-pulse conditions under which some Raman vibrations are frozen out. In addition, we note the approximate size of the $\chi^{(3)}$ tensor elements of the CaF_2 substrate, whose orientation is unknown.

Owyoung measured the rotation of the polarization ellipse of a beam of 694-nm, 10-ns pulses in fused quartz, relative to the rotation in CS_2.[10] This rotation is proportional to $c_{1221}(-\omega, \omega, \omega, -\omega)$, which is known to within a percent in CS_2 (through accurate determination of its Kerr constant). By this comparison he found $c_{1221}(-\omega, \omega, \omega, -\omega)$ to be 1.28×10^{-15} esu within ±7% in fused quartz. By measuring the polarized and the depolarized Raman spectra in fused quartz, Hellwarth *et al.* determined that ~6% of this value arises from the nuclear motions in fused quartz.[11]

The 110-fs pulses we have employed here are too short to be affected by Raman vibrations below 200 cm^{-1}.[12] A rough estimate of this freeze-out effect suggests that our pulses feel roughly half of the 6% Raman contribution. (More accuracy is not warranted.) Therefore we base our estimates of the absolute values of c_{1221} and c_{1122} for polycrystalline C_{60} on the value

$$c^q_{1221} = 1.24 \times 10^{-15} \text{ esu} \tag{18}$$

for fused quartz. Corrections for freeze-out effects and the ±7% absolute uncertainty in our quartz standard should be kept in mind in comparing our results to other experimental results on C_{60}. The entries (a, a), (b, b), (d, a), and (d, b) of Table 1 compare the two independent components of $\chi^{(3)}$ for fused quartz with the c_{1122} coefficient of C_{60}. From these we determine

$$c^q_{1122}/c^q_{1221} = 1.091 \pm 0.013. \tag{19}$$

This is 13% below the estimated ratio of 1.25 for long pulses.[12] For the purpose of estimating the absolute value of c_{1111} for C_{60}, we combine Eq. (18) with Eq. (19) to obtain

$$c^q_{1111} = (3.95 \pm 0.05) \times 10^{-15} \text{ esu} \tag{20}$$

as an appropriate reference value for our short pulses.

Using the standard quartz values above, we obtain the nonlinear tensor elements for polycrystalline C_{60} that appear in Eq. (10). These are given in Table 2 along with the data entries of Table 1 and relevant equations that were used to derive them. In quoting phase angles, we assume that the tensor elements of $\overleftrightarrow{\chi}(-\omega, \omega, \omega, -\omega)$ of both fused quartz and the CaF_2 substrate are real and positive. We find that the phase angles for all nonzero tensor components are the same within experimental accuracy.

Kajzar *et al.* saw two pronounced resonances in their measurements of third-harmonic generation versus wavelength (between 0.8 and 1.9 μm) in a C_{60} film. They observed a broad resonance at an incident wavelength of 1.3 μm, which they suggested is a two-photon resonance of the character that would produce a resonance in $\chi^{(3)}(-\omega, \omega, \omega, -\omega)$, also at 1.3 μm with a width of ~0.2 μm.[13] If we assume that this resonance dominates $\chi^{(3)}(-\omega, \omega, \omega, -\omega)$ at our wavelength of 768 nm, then a simple Lorentzian model for the resonance line predicts a phase angle for our $\chi^{(3)}$ elements near 160°, declining in value if a positive real background contribution to $\chi^{(3)}$ is

Table 2. Results for the Amplitudes and the Phases of the Third-Order Nonlinear Susceptibility Tensor $\chi^f(-\omega, \omega, \omega, -\omega)$ of C_{60} Obtained by Use of the Data of Table 1 in Eqs. (12)–(16) for the Optical Fields Generated in Beams 4, 5, and 6 in Fig. 1[a]

Quantity	Value
$\lvert c^f_{1122}/c^f_{1221}\rvert$	1.13 ± 0.05[b]
$\lvert c^f_{1111}\rvert$	$(1.42 \pm 0.03) \times 10^{-12}$ esu[c]
$\lvert \phi^f_{1111}\rvert$	(142° ± 5°)[d]
$\lvert c^f_{1122}\rvert$	$(0.50 \pm 0.01) \times 10^{-12}$ esu[e]
	$(0.49 \pm 0.01) \times 10^{-12}$ esu[f]
$\lvert \phi^f_{1122}\rvert$	(138° ± 10°)[g]
	(140° ± 12°)[h]
$\lvert c^f_{1221}\rvert$	$(0.44 \pm 0.03) \times 10^{-12}$ esu[i]
	$(0.44 \pm 0.01) \times 10^{-12}$ esu[j]
$\lvert \phi^f_{1221}\rvert$	(145° ± 17°)[k]

[a] Results are expressed in terms of the two independent tensor elements c^f_{1221} and c^f_{1122} defined in Eq. (10). The parallel-polarization element c^f_{1111} must equal $c^f_{1221} + 2c^f_{1122}$. For the determination of the phases ϕ^f_{ijkl} it is assumed that the nonlinear susceptibility in the CaF_2 substrate has a zero imaginary part. In the other footnotes to this table the symbol (a, b) refers to the data in row a and column b of Table 1.

[b] Average of the ratios of (a, a) to (a, b) and of (b, b) to (b, a), weighted by the inverse squares of their errors.

[c] Average of data entries (c, a) and (c, b), weighted by the inverse squares of their errors and substituted in Eqs. (12), (13), and (16).

[d] From data entry (c, d) interpreted by Eq. (14), with (c, c) giving the relative magnitudes of c^s_{xxxx}, presumed real and positive, in Eq. (15).

[e] Weighted average of values from entries (a, a) and (b, b).

[f] Values predicted by values superscripted (a) and (b) above and assuming $\phi^f_{1122} = \phi^f_{1221}$.

[g] From data entries (a, d), (a, a), and (a, c).

[h] From data entries (b, d), (b, b), and (b, c).

[i] Weighted average of values from entries (a, b) and (b, a).

[j] Value predicted by values superscripted (a) and (b) above.

[k] Value obtained from entry (d, d) in which $\lvert c^f_{1221}\rvert$ is obtained from the average of entries (d, a) and (d, b) divided by the square of the ratio superscripted (a) above.

added. Clearly our data support the existence of this resonance.

The magnitude of the c_{1111} value derived by us for the C_{60} film is the smallest value reported for this coefficient at any wavelength and a factor of 5 below the next nearest value reported by Lindle *et al.* at 1.06 μm.[14] Our value at 768 nm being lower is consistent with the two-photon resonance hypothesis. We find in addition that $|c_{1122}/c_{1221}| = 1.13 \pm 0.05$, which we have not yet interpreted.

The deviation of the tensor elements of the cubic CaF_2 substrate from isotropic symmetry is evident in column c of Table 1. Since we do not know the orientation of the cube axes, we cannot reconstruct this tensor. However, the substrate tensor elements appear not to deviate more than ~30% from the values of polycrystalline CaF_2, being ~70% of those of fused quartz. (See column c of Table 1.)

5. CONCLUSION

We have demonstrated an all-optical method that allows the measurement of the amplitude and the phase of all independent elements of the degenerate four-wave-mixing tensor of an isotropic thin film on a thick substrate. The method employs the interference of the degenerate four-wave-mixing signal from the substrate with that from the film, normalized to other signals generated by the same incident beams. Our observation of a negative real part in every element of $\chi^{(3)}$ at 768 nm of C_{60} supports the existence of a two-photon resonance, suggested by others to exist near 1.3 μm.

ACKNOWLEDGMENT

We acknowledge the support of this work through National Science Foundation grant DMR-9107806 and by the U.S. Air Force Office of Scientific Research.

REFERENCES

1. X. Zhang, X. Ye, and K. Chen, Opt. Commun. **113**, 519 (1995).
2. N. Tang, J. P. Partanen, R. W. Hellwarth, J. Laquindanum, L. R. Dalton, M. Q. He, and C. W. Spangler, Proc. SPIE **2285**, 186 (1994).
3. S. M. Saltiel, B. Van Wonterghem, and P. M. Rentzepis, Opt. Lett. **14**, 183 (1989).
4. M. L. Shand and R. R. Chance, J. Chem. Phys. **69**, 4482 (1978).
5. M. E. Orczyk, M. Samoc, J. Swiatkiewicz, N. Manickam, M. Tomoaia-Cotisel, and P. N. Prasad, Appl. Phys. Lett. **60**, 2837 (1992).
6. M. Sheik-Bahae, A. A. Said, T.-H. Wei, D. J. Hagan, and E. W. Van Stryland, IEEE J. Quantum Electron. **26**, 760 (1990).
7. P. D. Maker and R. W. Terhune, Phys. Rev. **137**, A801 (1965).
8. S. L. Ren, Y. Wang, A. M. Rao, E. McRae, J. M. Holden, T. Hager, K. Wang, W.-T. Lee, H. F. Ni, J. Selegue, and P. C. Eklund, Appl. Phys. Lett. **59**, 2678 (1991).
9. F. P. Strohkendl, D. J. Files, and L. R. Dalton, J. Opt. Soc. Am. B **11**, 742 (1994).
10. A. Owyoung, IEEE J. Quantum Electron. **QE-9**, 1064 (1973).
11. R. Hellwarth, J. Cherlow, and T.-T. Yang, Phys. Rev. B **11**, 964 (1975).
12. R. Hellwarth, Prog. Quantum Electron. **5**, 1 (1977).
13. F. Kajzar, C. Taliani, R. Zamboni, S. Rossini, and R. Danieli, Synth. Met. **54**, 21 (1993).
14. J. R. Lindle, R. G. S. Pong, F. J. Bartoli, and Z. H. Kafafi, Phys. Rev. B **48**, 9447 (1993).

Appendix II

Band Mobility of Photoexcited Electrons in $Bi_{12}SiO_{20}$

Ivan Biaggio,* Robert W. Hellwarth, and Jouni P. Partanen†

University of Southern California, Departments of Physics and Electrical Engineering, Los Angeles, California 90089-0484

(Received 10 May 1996)

We determine the band mobility of photoexcited electrons in cubic n-type $Bi_{12}SiO_{20}$. We measure a room-temperature mobility of 3.4 ± 0.5 cm^2/(V s) that decreases monotonically to 1.7 ± 0.3 cm^2/(V s) as the temperature is increased to 200 °C. We show that electrons in $Bi_{12}SiO_{20}$ form large polarons. Our results are predicted by strong coupling polaron theory if the band mass of the electrons is chosen to be 2.0 ± 0.1 electron masses. We determine the electron-phonon coupling constant and effective longitudinal optical phonon frequency required for this prediction from the available infrared reflectivity spectrum of $Bi_{12}SiO_{20}$. [S0031-9007(96)02214-4]

PACS numbers: 63.20.Kr, 42.70.Nq, 72.10.Di, 72.20.Fr

The mobility of a photoexcited electron drifting in the conduction band of transparent n-type cubic $Bi_{12}SiO_{20}$ crystals (n-BSO) at 300 K has been reported to lie between 3 and 5 cm^2/V s [1–3]. If the usual independent-collision model were used to describe this drift, the thermal mean free path (~0.2 nm) would be less than the de Broglie wavelength of the electron, and the collision rate times the Planck constant (the uncertainty in the electron energy) would be an order of magnitude greater than the thermal energy. In this "strong coupling" case the Boltzmann equation cannot be expected to apply. We report measurements of mobility vs temperature in n-BSO which can be explained well by a "polaron" theory that avoids the limitations of the Boltzmann equation [4–7].

An electron in a polar crystal polarizes the lattice in its neighborhood. The electron moving with its accompanying lattice distortion is called a polaron. We argue that a photoelectron in n-BSO constitutes the clearest case of a strongly coupled "large" polaron, i.e., a polaron whose wave function extends over many atoms, so that the electron can be thought of as interacting with phonons rather than with independent atoms. Previous examples of large polarons were found in a variety of alkali halides, where mobility values lie above ~12 cm^2/V s, the values for KCl and KBr at 330 °C [8]. These materials are closer to the case of independent collisions. Band mobilities lower than in n-BSO, like the value of 0.5 ± 0.1 cm^2/V s found in orthorhombic $KNbO_3$ [9], correspond to "small" polarons. Small polarons have a wave function extending less than an interatomic distance and move by hopping or tunneling [10]. Many even smaller mobility values are reported for various insulators, but these generally reflect the effects of shallow traps [1,11].

n-BSO has a sufficiently large linear electro-optic effect, so that charge separations can be easily seen. Therefore, we determine the electron mobility using the holographic time of flight (HTOF) method [9,11–14], in which two interfering laser beams excite a spatially sinusoidal pattern of charge carriers in the bulk of the sample. The evolution of this pattern is measured optically by observing the development of the space-charge-induced index change caused by the separation of the free carriers from their excitation point. HTOF techniques offer two distinct advantages over regular time-of-flight methods: (1) The length scale is set by the spatial period of the sinusoid and is easily varied. (2) The movement of the photoelectrons is measured optically, allowing a higher time resolution (given by the laser pulse length, which is 30 ps in our case). HTOF measurements can be performed in the presence of an applied electric field (*drift mode*) [13], or without any applied field (*diffusion mode*) [9,14], where purely thermal diffusion of the photoexcited charge distribution is measured. In this work we use the HTOF technique in diffusion mode, which has a number of additional advantages: (3) no electrodes are needed, (4) no particular sample shapes are required, and (5) no uncertainties are introduced because of possible internal electric field variations caused by trapped space charge.

The experimental four-wave-mixing configuration is shown in Fig. 1. We use a frequency-doubled Nd:YAG laser that produces 30 ps, 532 nm pulses at a repetition rate of 5 Hz. A beam splitter sends part of a pulse into a delay line, to act as a probe beam, and the other part is split again into two write pulses that arrive simultaneously in the sample. They excite a sinusoidal electron distribution, $\propto \sin(K_g z)$, from donor sites with energy levels near the middle of the 3.2 eV band gap into the conduction band. Their charge is compensated initially by that of the newly created ionized donor sites. Diffusion tends to make the conduction band electron distribution uniform, uncovering the space-charge field E_{sc} of photoionized donor sites with the following time dependence [13,14]:

$$E_{sc}(z,t) \propto [1 - \exp(-t/\tau)]\sin(K_g z), \qquad (1)$$

where $\tau^{-1} = \tau_0^{-1} + \tau_D^{-1}$. τ_0 is the average time for photoexcited electrons to remain in the conduction band before going to uniformly distributed traps of unknown origin. τ_D is the diffusion time,

$$\tau_D = \frac{e}{K_g^2 \mu k T}. \qquad (2)$$

0031-9007/97/78(5)/891(4)$10.00

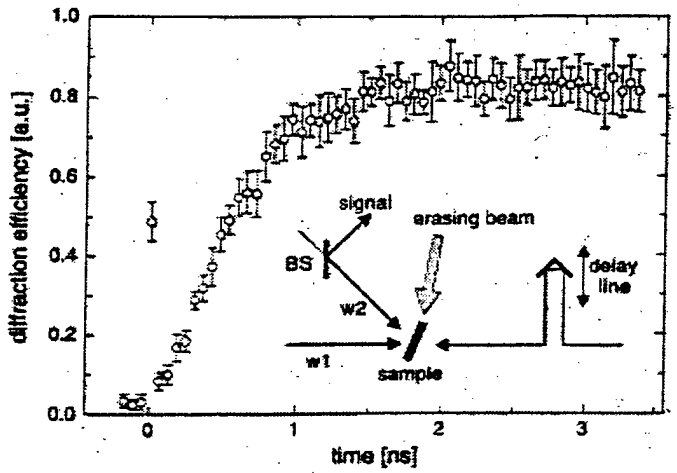

FIG. 1. Diffracted signal vs probe-pulse delay time in sample CT3, at a grating spacing of 0.38 μm. The inset shows the experimental arrangement. Two pulses w1 and w2 (532 nm, 30 ps) arrive in the sample at the same time. The probe pulse, which is counterpropagating to w1, is diffracted by the space-charge grating and produces a signal pulse counterpropagating to w2. The beam splitter BS sends the signal pulse into the detection system. The beam diameters are 1.7 mm for the write beams and 0.5 mm for the probe beam. All beams are vertically polarized. The grey arrow represents a cw erasing beam at 514 nm. It illuminates the crystal from the top with an intensity of approximately 0.1 W/cm^2.

Here e is the unit charge, K_g is the magnitude of the sinusoidal space-charge modulation wave vector, μ is the band mobility, k is Boltzmann's constant, and T is the absolute temperature. This analysis assumes that a small fraction of the donors are photoexcited, and that the evolution of the photoelectron pattern is dominated by diffusion, as justified experimentally below.

The space-charge field of (1) modulates the refractive index of the material via the linear electro-optic (Pockels) effect. We detect the resulting phase grating by diffracting the time-delayed probe pulse from it (see Fig. 1). We note that the buildup time of the space-charge field (1) does not depend on the write fluence [14], and that it is given by the diffusion time when it is much shorter than the free carrier lifetime. We know that photoexcitation of holes is not influencing our measurement, for, if hole transport were significant, we would not observe the time dependence in (1).

The sample is homogeneously illuminated all the time by a 514 nm argon ion laser beam with an intensity of approximately 0.1 W/cm^2. In the 0.2 s interval between two measurements, this illumination erases the space-charge induced grating created by the write pulses. During the measurement time (a few ns) the erase beam deposits 6 orders of magnitude less energy than the write pulses. We verified that it does not affect our results.

We use three nominally undoped n-BSO samples labeled SU1, CT1, and CT3. These crystals are well characterized by many experiments as described in Refs. [15,16]. The SU1 sample has been used in previous HTOF experiments in the drift mode [2,11,13].

The result of a typical measurement is shown in Fig. 1. When the probe pulse precedes the write pulse, there is only a small signal. A relatively strong signal caused by third order nonlinear effects is observed when the three pulses are present in the crystal at the same time. When the probe pulse is delayed (positive times in the figure), one sees the diffracted signal increase as the photoexcited electrons diffuse away from the positive ions at which they were bound, thus creating a space-charge field.

The signal observed before zero delay has amplitude E_0 and is due to scattered light from the probe pulse and to the remains of a grating that is not completely erased by the argon laser beam (scattered light from the write pulses was taken into account separately). Although it is very small, this background grating needs to be taken into account when measuring the buildup time. We fit the detected diffraction efficiency η to $\eta(t) \propto |E_{sc}(t) + E_0|^2$ by adjusting E_0 and τ [see (1)]. The relative phases of E_{sc} and E_0 are uncertain, especially at the low intensities where we performed the buildup time measurements. For each data set we perform two least squares fits: once imposing a phase shift of 90° between E_0 and E_{sc} and once imposing a 0 phase shift. To obtain a final value for the rise time, we average the results of the two fits, which differ by 20% at most.

In order to determine the mobility accurately, we must establish that we are in the low-fluence limit discussed above. To do this we measure the fluence dependence of both the buildup time and the magnitude of the signal. Figure 2(a) shows the grating amplitude and the buildup time τ as a function of write fluence in sample CT3. For small fluences, the grating amplitude grows linearly with the fluence of the write pulses, and the buildup time is a constant independent on fluence. As the write fluence F approaches 10 mJ/cm^2 saturation effects appear [9]. From the data in Fig. 2(a) one derives a photoexcitation cross section σ between $\sim 10^{-18}$ and 10^{-17} cm^2, consistent with an earlier estimate [15]. We performed all the mobility measurements described below with a write fluence of the order of 1 mJ/cm^2.

The dependence of the buildup times on grating spacing $2\pi/K_g$ is shown in Fig. 2(b). The data points were obtained by averaging several measurements. The buildup time is proportional to the square of the grating spacing. This confirms that the electron avoids shallow and deep traps for so long that the buildup time τ corresponds to the electron diffusion time τ_D and the grating buildup is dominated by diffusion [see (1), $\tau = \tau_D$]. The electron lifetime τ_0 in the SU1 sample has been independently determined to be 26 $\pm$ 2 ns [13]. The solid line in Fig. 2(b) is the result of a least-squares fit of (2) to the data of both samples, with only the mobility as a free parameter. It gives a mobility value of 3.4 $\pm$ 0.5 cm^2/Vs. The buildup times in the SU1 and CT3 samples are the same within the experimental error. This suggests that the

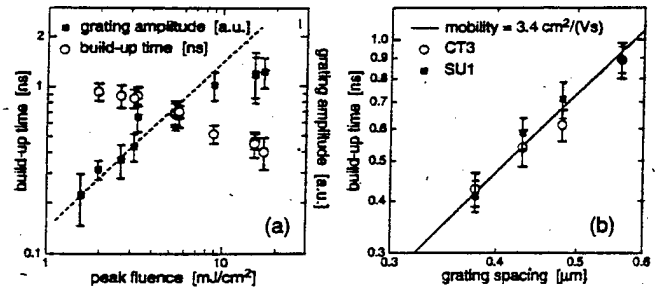

FIG. 2. (a) Grating buildup time and amplitude vs write pulse fluence in sample CT3 for a grating spacing of 0.56 μm. The dashed line gives a linear dependence of the grating amplitude on fluence. (b) Log-log plot of the grating buildup time τ vs grating spacing in samples SU1 and CT3 at 1 mJ/cm^2 fluence. The solid line is obtained from Eq. (2) using a mobility value of 3.4 cm^2/V s.

mobility is an intrinsic property of the material. This idea is also supported by our measurements in the CT1 crystal at the two largest grating spacings, where we found the buildup time to agree with the results in Fig. 2(b). Our mobility value is consistent with other, less accurate results reported previously [1–3]. A mobility of 50 cm^2/V s derived from grating buildup time in a similar experiment [17] is erroneous because trapping, not diffusion, dominated the dynamics [18].

Figure 3 shows the temperature dependence of the band mobility in CT3 and SU1. The sample was enclosed in a temperature-controlled oven with small apertures for the laser beams. We set up the experiment at room temperature and selected an appropriate write fluence around 1 mJ/cm^2 as described above. We raised the temperature, stopping every 20°-30° to stabilize it and perform a measurement. Care was taken not to change the adjustment of the experimental setup when changing the temperature of the crystal. The data in Fig. 3 were obtained at a grating spacing of 0.38 μm. Other measurements performed

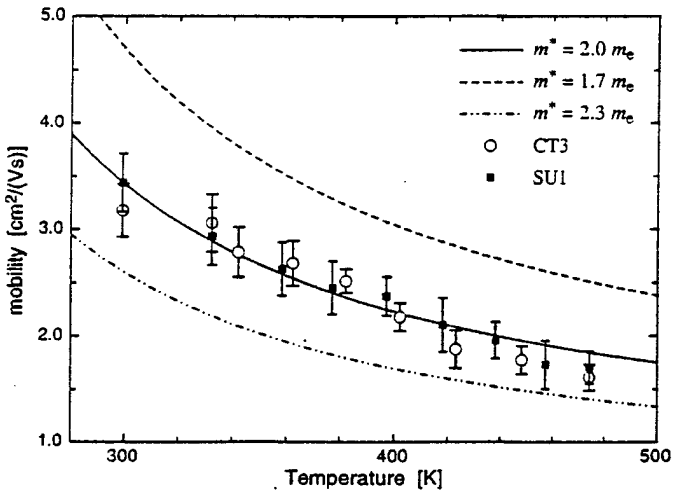

FIG. 3. Electron band mobility vs temperature in sample SU1 and CT3, and predictions of Eq. (4).

at longer grating spacings from 0.43 to 0.57 μm give the same temperature dependence, within experimental error.

The observed decrease of the mobility with rising temperature and the polar nature of the n-BSO lattice suggest that the band mobility is controlled by interaction with longitudinal optical (LO) phonons [4–7]. The interaction of an electron with a polarizable lattice has been studied in Refs. [5–7] starting from the "Fröhlich Hamiltonian" which has three material parameters: the electron-phonon coupling constant α, a single LO phonon frequency ν_{LO}, and the effective mass of the electron in the conduction band. In the alkali halide crystals where much of the polaron theory was applied [8], a single LO phonon frequency is appropriate. However, n-BSO has many polar optical vibrational branches with frequencies between 50 and 900 cm^{-1} [19]. In order to apply the extensive predictions of the existing polaron models [4–7] to our results, we have devised two mathematical schemes to imitate the phonon structure in n-BSO by a single "average" or "effective" LO phonon branch having frequency ν_{LO} Hz and oscillator strength W Hz. These are related by $(W^2/\nu_{LO}^2) = \epsilon_\infty^{-1} - \epsilon_{dc}^{-1}$. Here $\epsilon_\infty = 5.7$ is the long wavelength limit of the electronic contribution to the refractive index squared, and $\epsilon_{dc} = 50$ is the clamped dc dielectric constant. Our schemes determine ν_{LO} and W from the experimental infrared reflectivity spectrum of n-BSO at room temperature [19]. In terms of ν_{LO} and W, the dimensionless coupling constant α defined by Fröhlich is

$$\alpha = (W/\nu_{LO})^2\,(\mathrm{Ry}/h\nu_{LO})^{1/2}\,(m^*/m_e)^{1/2}, \qquad (3)$$

where Ry = 13.6 eV is one Rydberg of energy, h is Planck's constant, m^* is the effective mass of an electron in the conduction band (with no phonons), and m_e is the electron mass. Using the frequency dependence of the dielectric constant of n-BSO we obtain, from one scheme, $W/c = 195$ cm^{-1} and $\nu_{LO}/c = 504$ cm^{-1}, and thus a coupling constant $\alpha = 2.25\sqrt{m^*/m_e}$. A second scheme gives $W/c = 195$ cm^{-1} and $\nu_{LO}/c = 495$ cm^{-1} instead, which makes negligible difference in the predictions.

Since our experiment was performed above room temperature, we use the general result [Eqs. (46) and (47)] of Ref. [7], obtained before the low temperature limit was taken,

$$\frac{e}{2\pi\nu_{LO}m^*}\,\mu^{-1} = \frac{\alpha}{3\sqrt{\pi}}\,\frac{\beta^{5/2}}{\sinh(\beta/2)}\,\frac{v^3}{w^3}\,K(a,b), \qquad (4)$$

where μ is the mobility, $\beta \equiv h\nu_{LO}/kT$, $K(a,b) \equiv \int_0^\infty du\cos(u)/[u^2 + a^2 - b\cos(vu)]^{3/2}$, $a^2 \equiv (\beta/2)^2 + R\beta\coth(\beta v/2)$, $b \equiv R\beta/\sinh(b\beta v/2)$, $R \equiv (v^2 - w^2)/w^2 v$, and v, w are temperature dependent variational parameters [5,6]. We find that putting $b = 0$ in (4) makes less than 0.1% error throughout our temperature range. This is useful because $K(a,0) = K_1(a)/a$, where K_1 is a modified Bessel function [20]. We note that (4),

TABLE I. Variational parameters v and w for various coupling constants α and temperature parameters β.

	$\alpha = 2$		$\alpha = 3$		$\alpha = 4$	
	v	w	v	w	v	w
$\beta = 1.5$	5.52	4.29	6.02	4.01	6.66	3.70
$\beta = 2.0$	4.48	3.40	4.94	3.16	5.54	2.88
$\beta = 2.5$	3.89	2.93	4.32	2.70	4.90	2.45

where $K_1(a)/a$ can be substituted for $K(a, b)$, becomes equal to Eq. (24) in Ref. [21] in the limit of small α.

We determined the parameters v and w at every temperature by following the free energy minimization procedure described in Ref. [6]. Table I gives the values of the v, w parameters in the temperature range we investigated. Using these values we estimate a polaron radius of approximately 0.6 nm [22]. The n-BSO unit cell is 1.0 nm large and contains 66 atoms. The sphere defined by the polaron radius contains ~60 atoms. Therefore, the continuum approximation of Refs. [5–7] can be applied.

The only unknown parameter in (3) and (4) is the electron effective band mass m^*. The prediction of (4) at $T = 300$ K corresponds to our room-temperature mobility value of 3.4 cm^2/Vs when setting $m^* = 2.01m_e$. From m^* and (4) we can predict the temperature dependence of the mobility. The result is shown in Fig. 3 together with two other curves obtained using $m^* = 1.7m_e$ and $m^* = 2.3m_e$. The agreement with the $m^* = 2.0m_e$ curve is very good. No parameter was adjusted to fit the experimental temperature dependence, which is given mostly by the effective phonon frequency ν_{LO}.

In conclusion, we have presented comparative and thermal evidence that photoelectrons in nominally undoped, n-type $Bi_{12}SiO_{20}$ are large, strongly coupled polarons; their observed band mobility is intrinsic. Their small mobility makes photoelectrons in n-type $Bi_{12}SiO_{20}$ the clearest example of such polarons.

We would like to acknowledge the support of the Air Force Office of Scientific Research under Grant No. F49620-94-1-0139.

*Permanent address: Nonlinear Optics Laboratory, Institute of Quantum Electronics, Swiss Federal Institute of Technology, ETH-Hönggerberg, CH-8093 Zürich.

†Also with 3D Systems, 26081 Avenue Hall, Valencia, CA 91355.

[1] G. Le Saux and A. Brun, IEEE J. Quantum Electron. **QE-23**, 1680 (1987); P. Nouchi, Ph.D. dissertation, University of Southern California, Los Angeles, 1992; P. Nouchi, J. P. Partanen, and R. W. Hellwarth, Phys. Rev. B **47**, 15 581 (1992).

[2] P. Nouchi, J. P. Partanen, and R. W. Hellwarth, in *Conference on Lasers and Electro-Optics, 1992*, OSA Technical Digest Series Vol. 12 (Optical Society of America, Washington, D.C., 1992), p. 84.

[3] S. L. Sochava, K. Buse, and E. Krätzig, Phys. Rev. B **51**, 4684 (1995).

[4] H. Fröhlich, Adv. Phys. **3**, 325 (1954).

[5] R. P. Feynman, Phys. Rev. **97**, 660 (1955).

[6] Y. Osaka, Prog. Theor. Phys. **22**, 437 (1959).

[7] R. P. Feynman, R. W. Hellwarth, C. K. Iddings, and P. M. Plazman, Phys. Rev. **127**, 1004 (1962).

[8] F. C. Brown, in *Point Defects in Solids*, edited by J. H. Crawford and L. M. Slifkin (Plenum Press, New York, London, 1972), Chap. 8.

[9] M. Ewart, I. Biaggio, M. Zgonik, and P. Günter, Phys. Rev. B **49**, 5263 (1994).

[10] D. Emin, Phys. Today **35**, No. 6, 34 (1982).

[11] P. Nouchi, J. P. Partanen, and R. W. Hellwarth, J. Opt. Soc. Am. B **9**, 1428 (1992).

[12] G. Pauliat, A. Viling, J. C. Launay, and G. Roosen, J. Opt. Soc. Am. B **7**, 1481 (1990).

[13] J. P. Partanen, J. M. C. Jonathan, and R. W. Hellwarth, Appl. Phys. Lett. **57**, 2404 (1990); J. P. Partanen, P. Nouchi, J. M. C. Jonathan, and R. W. Hellwarth, Phys. Rev. B **44**, 1487 (1991).

[14] I. Biaggio, M. Zgonik, and P. Günter, J. Opt. Soc. Am. B **9**, 1490 (1992).

[15] Ping Xia, J. M. C. Jonathan, J. P. Partanen, and R. W. Hellwarth, Opt. Lett. **18**, 1780 (1993).

[16] F. P. Strohkendl, P. Tayebati, and R. W. Hellwarth, J. Appl. Phys. **66**, 6024 (1989).

[17] J. M. C. Jonathan, G. Roosen, and P. Roussignol, Opt. Lett. **13**, 224 (1988).

[18] G. Pauliat and G. Roosen, J. Opt. Soc. Am. B **7**, 2259 (1990).

[19] W. Wojdowski, T. Lukasiewicz, W. Nazarewicz, and J. Zmlja, Phys. Status Solidi (b) **94**, 649 (1979).

[20] M. Abramowitz and I. A. Stegun, *Handbook of Mathematical Functions* (Dover Publications, Inc., New York, 1972).

[21] K. K. Thornber and R. P. Feynman, Phys. Rev. B **1**, 4099 (1959).

[22] T. D. Schultz, Phys. Rev. **116**, 526 (1959).